

High-Index Faceted Noble Metal Nanocrystals

ZEWI QUAN,[†] YUXUAN WANG,[‡] AND JIYE FANG*,^{†,‡}

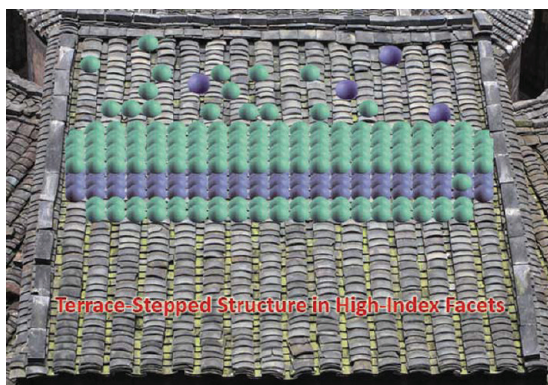
[†]Department of Chemistry and [‡]Materials Science and Engineering Program,
State University of New York at Binghamton, Binghamton, New York 13902,
United States

RECEIVED ON NOVEMBER 15, 2011

CONSPECTUS

The formation of novel and complex structures with specific morphologies from nanocrystals via a direct assembly of atoms or ions remains challenging. In recent years, researchers have focused their attention on nanocrystals of noble metals and their controlled synthesis, characterization, and potential applications. Although the synthesis of various noble metal nanocrystals with different morphologies has been reported, most studies are limited to low-index facet-terminated nanocrystals. High-index facets, denoted by a set of Miller indices $\{hkl\}$ with at least one index greater than unity, possess a high density of low-coordinated atoms, steps, edges, and kinks within these structures and serve as more active catalytic sites. With the potential for enhanced catalytic performance, researchers have used the insights from shape-controlled nanocrystal synthesis to construct noble metal nanocrystals bounded with high-index facets. Since the report of Pt tetrahedral nanocrystals, researchers have achieved significant progress and have prepared nanocrystals with various high-index facets. Because of the general order of surface energy for noble metals, high-index facets typically vanish faster in a crystal growth stage and are difficult to preserve on the surface of the final nanocrystals. Therefore researchers have had limited opportunities to examine high-indexed noble metal nanocrystals with a controlled morphology and investigate their resultant behaviors in depth.

In this Account, we thoroughly discuss the basic concepts and state-of-the-art morphology control of some noble metal nanocrystals enclosed with high-index facets. We briefly introduce high-index facets from both crystallographic and geometrical points of view, both of which serve as methods to classify these high-index facets. Then, we summarize various typical noble metal nanocrystals terminated by different types of high-index facets, including $\{hk0\}$ ($h > k > 0$), $\{hhl\}$ ($h > l > 0$), $\{hkk\}$ ($h > k > 0$), and $\{hkl\}$ ($h > k > l > 0$). In each type, we describe several distinct morphologies including convex, concave, and other irregular shapes in detail. Based on these remarks, we discuss key factors that may induce the variations of Miller indices in each class, such as organic capping ligands and metallic cationic species. In a look at applications, we review several typical high-indexed noble metal nanocrystals showing enhanced electrocatalytic or chemical catalytic activities.



1. Introduction

Ruthenium (Ru), rhodium (Rh), palladium (Pd), silver (Ag), osmium (Os), iridium (Ir), platinum (Pt), and gold (Au) are usually considered noble metals, which are defined as metals that are resistant to corrosion and oxidation in moist air. Noble metals are used everywhere, from household items to industry applications, due to their distinctive properties such as enhanced strength and toughness, excellent thermal and electrical conductivity, and high melting points.¹ Among them, catalysts composed of noble metals (especially Pd, Pt, and Au) are of technological importance

and are indispensable in diverse areas such as modern chemical industry, automotive exhaust purification, fuel cells, and gas sensors.² Due to their rare reserves on the earth, improvement of the intrinsic catalytic performance and the utilization efficiency of noble metals is still an interesting topic.

When the dimension of noble metal catalysts is reduced to nanoscale (designated as "nanocatalysts"), their surface-to-volume ratio would be dramatically increased. This may result in an enhancement of their electrocatalytic efficiency and a reduction of the cost.³ Recent development of

nanotechnology has enabled the success of noble metal nanocatalyst preparation with controllable composition, size, and shape.^{4–9} For example, it was reported that catalytic activity of bulk bimetallic Pt–M electrocatalysts (M = V, Ti, Co, Fe, Ni, ...) could be significantly improved^{12,13} with strong resistance to poisonous substances¹⁴ in comparison with Pt. Accordingly, nanometer-sized Pt–M alloys with tunable compositions have attracted increasing attention to develop.^{10–14} It was also reported that a single-crystal metal surface with open structures usually exhibits superior performances as model catalysts.^{3,20–22} More recently, many research efforts are being devoted to the investigation of noble metal nanocrystals (NCs) on a correlation between the electrocatalytic properties and surface crystal structure (determined by shape), because the electrocatalytic characteristics including activity, selectivity, and stability are strongly dependent on their surface atomic arrangement and configuration associated with terraces, steps, kinks, and vacancies. When a noble metal/alloy is “transferred” from bulk to nanophase, crystal-facet-dependent study (especially the high-index facets) becomes more significant and essential.

High-index facets, which are denoted by a set of Miller indices $\{hkl\}$ with at least one index being greater than unity, are considered as one kind of open structures. These facets possess a high density of low-coordinated atoms such as steps, edges, and kinks, serving as catalytically more active sites.¹⁵ As a result, noble metal catalysts with high-index planes usually exhibit significantly enhanced activities compared with those close-packed low-index facets such as (100) planes. Consequently, high-indexed noble metal NCs, which are the subject of this Account, can combine the advantages of both nanocatalysts and high-index facets and are expected to possibly serve as a new generation of catalysts. Since the surface energy of noble metals generally follows the order of $\gamma_{\{111\}} < \gamma_{\{100\}} < \gamma_{\{110\}} < \gamma_{\{hkl\}}$,^{3,16} high-index facets normally grow faster during a growth stage and thus are preferentially eliminated to minimize total surface energies of the final NCs. In order to experimentally evaluate the “collective” behavior of a specific nanocrystalline facet, it is essential to synthesize various nanometer-sized polyhedra ideally terminated with a single type of crystal facet (hereafter “nanopolyhedra”). Apparently, it is a challenge to produce high-indexed noble metal nanopolyhedra, as seen by the development timeline of noble metal NCs. It has been more than 150 years since Au colloids were prepared in a solution-phase approach by Faraday.¹⁷ Shape-controlled uniform metal NCs had not been achieved until 1996, when El-Sayed et al. demonstrated a preparation of Pt nanocubes

and nanotetrahedra.¹⁸ Thereafter, there have been myriad reports on development of controlled synthesis of noble metals NCs, although the NC surfaces were dominated by low-index facets in most literature. Since a preparation of high-indexed Pt NCs by Sun et al. in 2007,¹⁹ exploration of high-indexed noble metal nanopolyhedra has increased, especially in recent years.

2. Identification of High-Index Facets

To illustrate a direct relationship between polyhedral profile and surface plane, a triangular graph is presented in Figure 1A.²⁰ In this graph, three vertices represent three typical polyhedra encased by low-index facets: cube with 6 $\{100\}$ facets, octahedron with 8 $\{111\}$ facets, and rhombic dodecahedron with 12 $\{110\}$ facets. Among them, the $\{100\}$ and $\{111\}$ planes are atomic-scale flat with closely packed surface, whereas the $\{110\}$ planes are rough with stepped atoms. In contrast, polyhedra staying in three sidelines and interior of the triangle represent four types of high-indexed polyhedra, that is, tetrahedra (THH), trapezohedra (TPH), trisoctahedra (TOH), and hexoctahedra (HOH). In each polyhedron, the exposed facets have a strong correlation with the polyhedron type. For example, THH are bounded by 24 $\{hkl\}$ ($h > k > l = 0$) facets, TPH by 24 $\{hkl\}$ ($h > k = l > 0$), TOH by 24 $\{hkl\}$ ($h = k > l > 0$), and HOH by 48 $\{hkl\}$ ($h > k > l > 0$) facets, which are, afterward, denoted as $\{hk0\}$, $\{hkk\}$, $\{hhl\}$, and $\{hkl\}$, respectively. Such an increased number of facets in high-indexed polyhedra indicate an elevated percentage of edge and corner sites in these polyhedra (more rough). In each type, the Miller indices of the high-index facet are directly correlative with the geometrical parameters of the polyhedron. A high-indexed polyhedron staying in each sideline could be geometrically viewed as integration of two low-indexed polyhedra locating at both ends of its sideline. For example, THH is an integration between cube and rhombic dodecahedron, TOH is between octahedron and rhombic dodecahedron, and TPH is between cube and octahedron. It is very helpful to correlate it with a microfacet notation method, which will be discussed in next paragraph. Additionally, there is another way to intuitively describe these high-indexed polyhedra. Taking THH as an example, it can be deemed as a cube with each face capped by a square pyramid, which is obtained from a cube by “pulling out” the centers of its six square facets. Similarly, “pulling out” the centers of triangular facets in an octahedron forms eight triangular pyramids, which is a TOH. All of the profiles presented in this triangle are considered as **convex** polyhedra. In contrast to them, **concave**

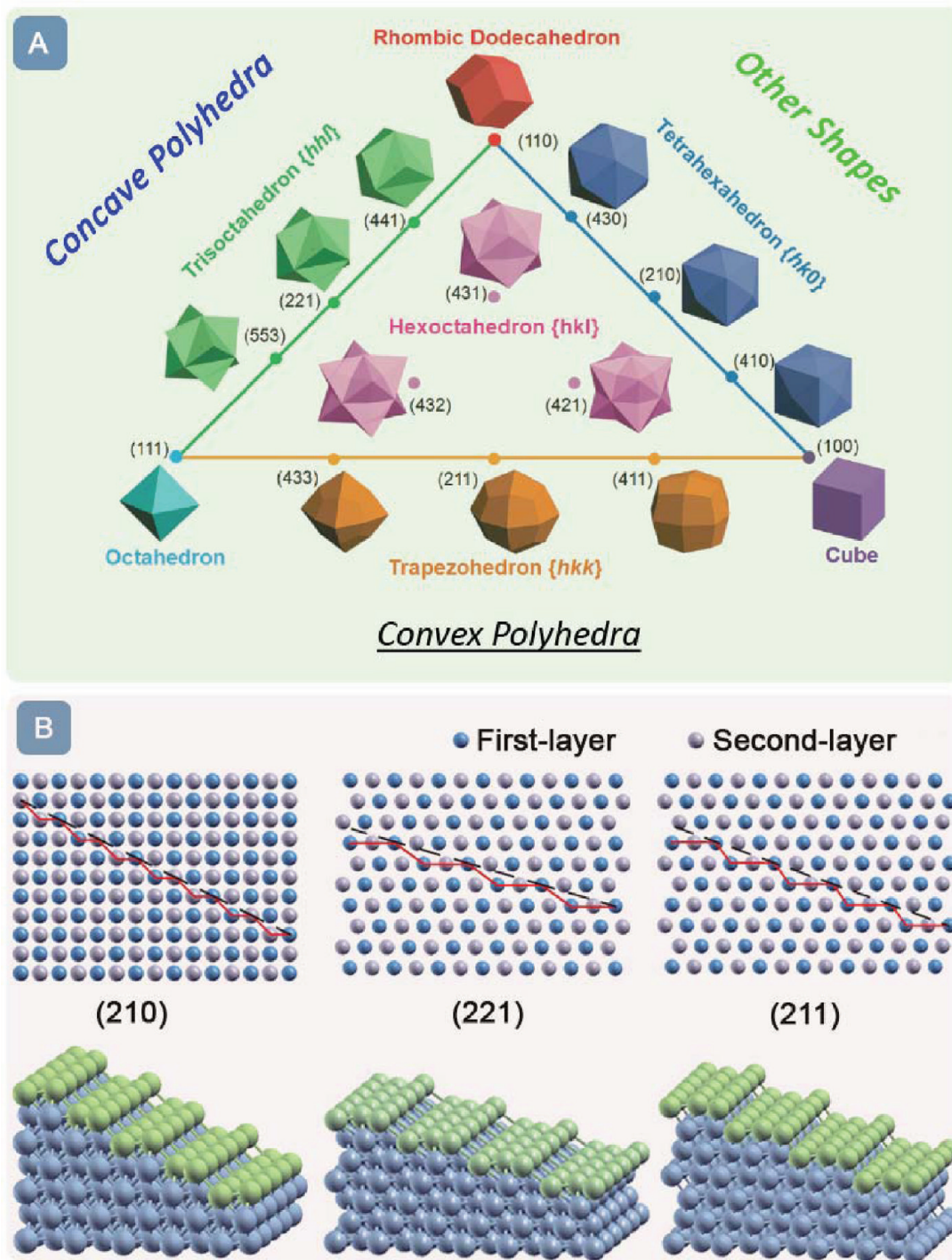
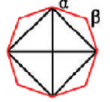
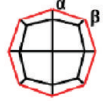

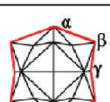


FIGURE 1. (A) Unit stereographic triangle of polyhedral NCs enclosed by different types of crystalline facets and (B) 2D and 3D atomic models of three typical high-index facets terminated with (210), (221), and (211) planes, respectively. Panel A adapted with permission from ref 20. Copyright 2010 American Chemical Society.

polyhedra enclosed by the same group of high-index facets are also achievable by “pushing in” centers of the corresponding surfaces. For example, a concave cube could be viewed as a cube with centers of the six square faces “pushed in” to generate square pyramid-shaped depressions. It should be pointed out that all the surfaces of these

polyhedra are exclusively composed of similar high-index facets regardless of the curvature of polyhedra (convex or concave). As a special group of high-indexed polyhedra, **other shapes** of which surfaces are partially bounded by high-index facets (usually in side surface) are also attracting attention. As a result, three types of these high-indexed

TABLE 1. Crystallographic Details of Four Types of High-Indexed Nanopolyhedra and the Projection Method To Determine Their Miller Indices

High-indexed polyhedron	Zone	Surface facets	Miller index ($n \geq 2$)	Microfacet notation	Projection direction	Projection image	Projection angle /degree
Tetrahexahedron (THH)	[001]	$\{hk0\}_{24}$ ($h > k > 0$)	($n, n-1, 0$)	$n(110) \times (100)$	[001]		$\alpha = 2 \arctan\left(\frac{h}{k}\right)$ $\beta = 270 - \alpha$
			($n, 1, 0$)	$n(100) \times (110)$			
Trapezohedron (TPH)	$[01\bar{1}]$	$\{hkk\}_{24}$ ($h > k > 0$)	($n+1, n-1, n-1$)	$n(111) \times (100)$	[001]		$\alpha = 2 \arctan\left(\frac{h}{k}\right)$ $\beta = 270 - \alpha$
			($2n-1, 1, 1$)	$n(100) \times (111)$			
Trisoctahedron (TOH)	$[1\bar{1}0]$	$\{hhl\}_{24}$ ($h > l > 0$)	($n+1, n+1, n-1$)	$n(111) \times (110)$	[110]		$\alpha = 2 \arctan\left(\frac{\sqrt{2}h}{n-1}\right)$ $\beta = 90 - (\alpha/2) - (\gamma/2)$ $\gamma = 2 \arctan\left(\frac{\sqrt{2}h}{l}\right)$
			($2n-1, 2n-1, 1$)	$n(110) \times (111)$			
Hexoctahedron (HOH)		$\{hkl\}_{48}$ ($h > k > l > 0$)			[110]		$\alpha = 2 \arctan\left(\frac{\sqrt{2}h}{n-1}\right)$ $\beta = 90 - (\alpha/2) - (\gamma/2)$ $\gamma = 2 \arctan\left(\frac{k+h}{\sqrt{2}l}\right)$

noble metal nanopolyhedra classified by their surface facet nature are included in this Account.

To better understand these high-index facets, as typical examples, four types of convex polyhedra are listed in the left part of Table 1. THH, TOH, and TPH staying in three sidelines correspond to [001], $[01\bar{1}]$, and $[1\bar{1}0]$ crystallographic zones, in which the planes exhibit characteristic terrace-step structure and are thus called stepped surfaces as well. A microfacet notation was developed to straightforwardly denote these stepped surfaces. It was first introduced by Lang, Joyner, and Somorjai to visualize stepped structure on Pt high-index facets.²¹ This notation has a general form $n(h_t k_t l_t) \times (h_s k_s l_s)$, meaning n atomic width of $(h_t k_t l_t)$ terraces separated by monatomic $(h_s k_s l_s)$ steps.^{2,22} According to Table 1, it is easy to obtain an appropriate microfacet expression for a given high-index facet. For example, (410) facets on THH can be expressed as $4(100) \times (110)$, indicating a stepped surface composed of a terrace in four atomic width of (100) symmetry, separated by a monatomic step of (110) symmetry. Likewise, (221) facets on TOH, which is actually (442), a designation $3(111) \times (100)$ shows that three-atom-width (111) terraces are separated by single-height (100) steps. Taking (210), (221), and (211) as representative examples, Figure 1B shows both their two-dimensional (2D) and their three-dimensional (3D) atomic models, clearly demonstrating the terrace-step structures. Technically, an accurate identification of surface planes exposed on high-indexed polyhedra is still a challenge. As one approach, the surface atomic arrangement obtained from a high-resolution transmission electron microscopy (HR-TEM) image in

conjunction with a microfacet illustration, can be used to determine Miller indices of high-index facets (method 1). However, it is not always possible to collect explicit information of surface atom arrangements, depending on many factors such as polyhedron orientation, surface ligand contamination, and technical limitation. As illustrated in the right part of Table 1, there is another relatively simple and efficient way to identify the surface indices using a projection angle measured along an appropriate crystallographic axis (method 2): [001] is the optimal projective direction for THH and TPH, while $[110]$ is optimal for TOH and HOH. In this way, octagons with 4-fold rotation symmetry are generated for THH and TPH cases, in which two angles, α and β along $\langle 100 \rangle$ and $\langle 110 \rangle$ directions, can be used to identify the high-index facets via appropriate equations. Similarly, the projections for TOH and HOH are octagons with 2-fold rotation symmetry, in which three angles, α , β , and γ along $\langle 100 \rangle$, $\langle 110 \rangle$, and $\langle \bar{1}10 \rangle$ directions, are dependent on their Miller indices. Consequently, Miller indices of high-index facets on a polyhedron could be determined by measuring the angles in an appropriate projection in comparison with the calculated values. In the following section, case studies on noble metal nanopolyhedra terminated with various high-index facets using above-mentioned method(s) are provided.

3. Case Studies

3.1. $\{hk0\}$ Facets. By treating polycrystalline Pt spheres with a square wave potential, Pt THH NCs exclusively covered by $\{hk0\}$ facets were successfully prepared,¹⁹ and their SEM images are illustrated in Figure 2A1–A6. Plane

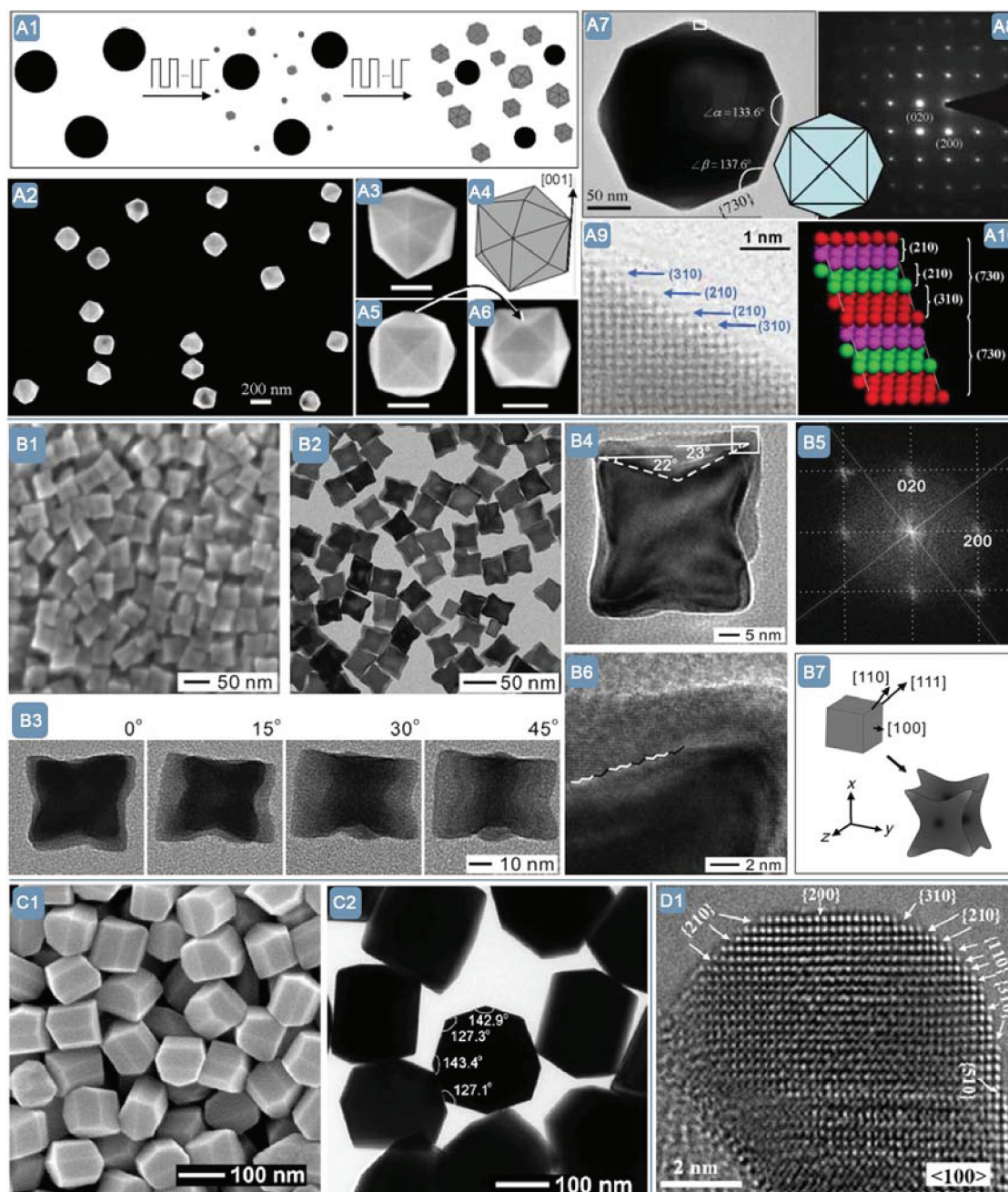


FIGURE 2. Typical cases of $\{hk0\}$ facets: (A1) formation scheme and (A2, A3, A5, A6) SEM images of Pt THH NCs at different magnifications and orientations, (A4) geometrical model of an ideal THH, and (A7) TEM image, (A8) SAED pattern, (A9) HR-TEM image, and (A10) 3D atomic model of Pt $\{730\}$ plane; (B1) SEM image, (B2–B4) TEM images, (B5) FT pattern, (B6) HR-TEM image, and (B7) formation scheme of Pd concave cubes; (C1) SEM and (C2) TEM images of Au truncated DTPs; (D1) HR-TEM image of Pt/C nanocatalysts along $\langle 100 \rangle$ axis. (A) Adapted with permission from ref 19. Copyright 2007 American Association for the Advancement of Science. (B) Adapted with permission from ref 29. Copyright 2011 Wiley. (C) Adapted with permission from ref 34. Copyright 2011 American Chemical Society. (D) Adapted with permission from ref 38. Copyright 2010 Wiley.

angles between two adjacent facets parallel to the $[001]$ zone axis were measured on the basis of the aforementioned method 2 (Figure 2A7,A8), and Miller indices of the exposed surfaces were therefore determined to be $\{730\}$ facets. Such a high-index facet is actually a periodical combination of two (210) facets and one (310) facet. This

assignment was further confirmed by HR-TEM image (method 1), which is in a good agreement with the 3D atomic model of $\{730\}$ facets (Figure 2A9,A10). Interestingly, if the square wave potential preparation strategy was applied to a Pd system, Pd nanorods bounded by $\{hk0\}$ or $\{hkk\}$ facets rather than Pd THH NCs could be harvested, even if Pd

exhibits similar electrochemical properties to Pt such as potential-induced oxygen adsorption and desorption.²³ Shortly, Pd THH NCs were generated on a glassy carbon electrode through a modified electrodeposition method,²⁴ and their surface planes were characterized as {730} facets, supported by HR-TEM image and selected area electron diffraction (SAED) pattern (method 1).

With some limitations such as scale-up difficulty in the electrochemical approach, high-index facet terminated NCs were alternatively prepared via a solution strategy. In 2008, Xie et al. reported a solution-phase synthesis of {221}-bounded Au TOH NCs (*vide infra*).²⁵ Since then, the solution method has blossomed and noble metal NCs with various kinds of high-index facets have been successfully synthesized. As an example of the {*hk0*} class, Au NCs enclosed by {730} facets were prepared by Wang et al. in 2009²⁶ using a seed-mediated growth approach that was originally proposed by El-Sayed²⁷ and Murphy.²⁸ Another class of {*hk0*} nanopolyhedra, concave nanocubes, has recently been synthesized from an aqueous solution.^{29,30} Based on SEM and TEM observation (Figure 2B1–B3), each face of the Pd nanocube was excavated by a square pyramid in the center, generating concave nanocubes (reversed THH). Further analysis (Figure 2B4–B6) revealed that the exposed surfaces could also be indexed to {730} facets (methods 1 and 2). It should be noted that such high-index facets (Figure 2B7) were achieved by a selective deposition of Pd atoms onto edges and corners (rather than surfaces) through a careful manipulation of reduction kinetics.²⁹ It was reported that in the solution approach a capping ligand can play a significant role, such as selectively binding to some specific facets, thus altering the relative growth rates perpendicular to various crystallographic planes and making high-indexed nanopolyhedron thermodynamically favorable. For example, in contrast to Au THH prepared in the presence of cetyltrimethylammonium bromide (CTAB), Au concave nanocubes bounded by {720} facets were obtained if CTAB was replaced by cetyltrimethylammonium chloride (CTAC) while the rest of the reaction conditions were kept identical.³¹ Metallic cationic species can also steer a formation of high-index metal NCs. For instance, Ag⁺ has been widely used to produce high-indexed Au NCs such as Au THH²⁶ and concave nanocubes,³¹ through an underpotential deposition (UPD) mechanism,³² in which a reduction of up to a monolayer of Ag onto an existing Au surface is involved. Such a Ag monolayer, similar to organic surfactants, may selectively bind to some specific facets to facilitate the final NC shape. More interestingly, Mirkin et al. recently demonstrated that

different facets can be selectively stabilized by utilizing different concentrations of Ag⁺ in a seed-mediated synthesis.³³ Such a manipulation was utilized to prepare four classes of different nanopolyhedra including {111}-terminated octahedra, {110}-bounded rhombic dodecahedra, {310}-enclosed truncated ditetragonal prisms (DTP), and {720}-faceted concave cubes.³³ In addition to a single class of Ag⁺ ions, a synergistic effect of two foreign metal ionic species, Ag⁺ and Pd²⁺, was also used on shape-selective synthesis of high-indexed Au NCs.³⁴ Among them, truncated DTP, as a class of novel nanopolyhedra enclosed by {*hk0*} facets, is shown in Figure 2C1,C2, the surfaces of which were determined as {310} via method 2.³⁴ It should be mentioned that due to their extensive study, high-indexed Au NCs were also used as templates to heteroepitaxially grow Au (core)–M (shell) (M = Pt, Pd, ...) nanopolyhedra. For example, THH,³⁵ cubes,³⁶ and TOH²⁰ of Au NCs, as core seeds, have been employed to direct the growth of bimetallic core–shell THH NCs.

In addition to THH, concave nanocubes, and truncated DTP, there are many other types of NCs that are bounded by {*hk0*} facets such as Pt multiple twinned nanorods³⁷ and Pd nanorods with decagonal pyramids.²³ Recently, it was reported that small Pt nanoparticles (NPs, 2–10 nm) supported on carbon black were composed of multiple {*hk0*} facets.³⁸ As shown in Figure 2D1, aberration-corrected HR-TEM images along the <100> axis reveals an atomically resolved border, on which a high density of low-coordinate atomic steps, such as {110}, {210}, {310}, and {510} steps, can be identified.

3.2. {*hhl*} Facets. As a successful example in solution-phase synthesis of high-indexed nanopolyhedra, Au TOH NCs with a size of larger than 100 nm were first prepared in 2008, and their surface planes were ascribed to 24 {221} facets.²⁵ Subsequently, Au TOH NCs with customizable size from 55 to 120 nm were developed by Lee and co-workers.³⁹ Analysis of the projection angles (method 2) and the atomic arrangement in the edge-on facets (method 1) shown in Figure 3A1–A3 indicates that their surfaces are bounded by high-index {*hhl*} facets, such as {221}, {331}, or {441}. Taking {221} as an example, it can be described as 3(111) × (110) based on microfacet expression, in which the atomic arrangement is periodic with three atomic widths of (111) terraces, followed by one atomic width of a (110) step (Figure 3A3).

Like Au THH, Au TOH NCs have also been used as templates to facilitate high-indexed nanopolyhedra via epitaxial growth.^{20,35} Wang et al. prepared Au–Pd core–shell

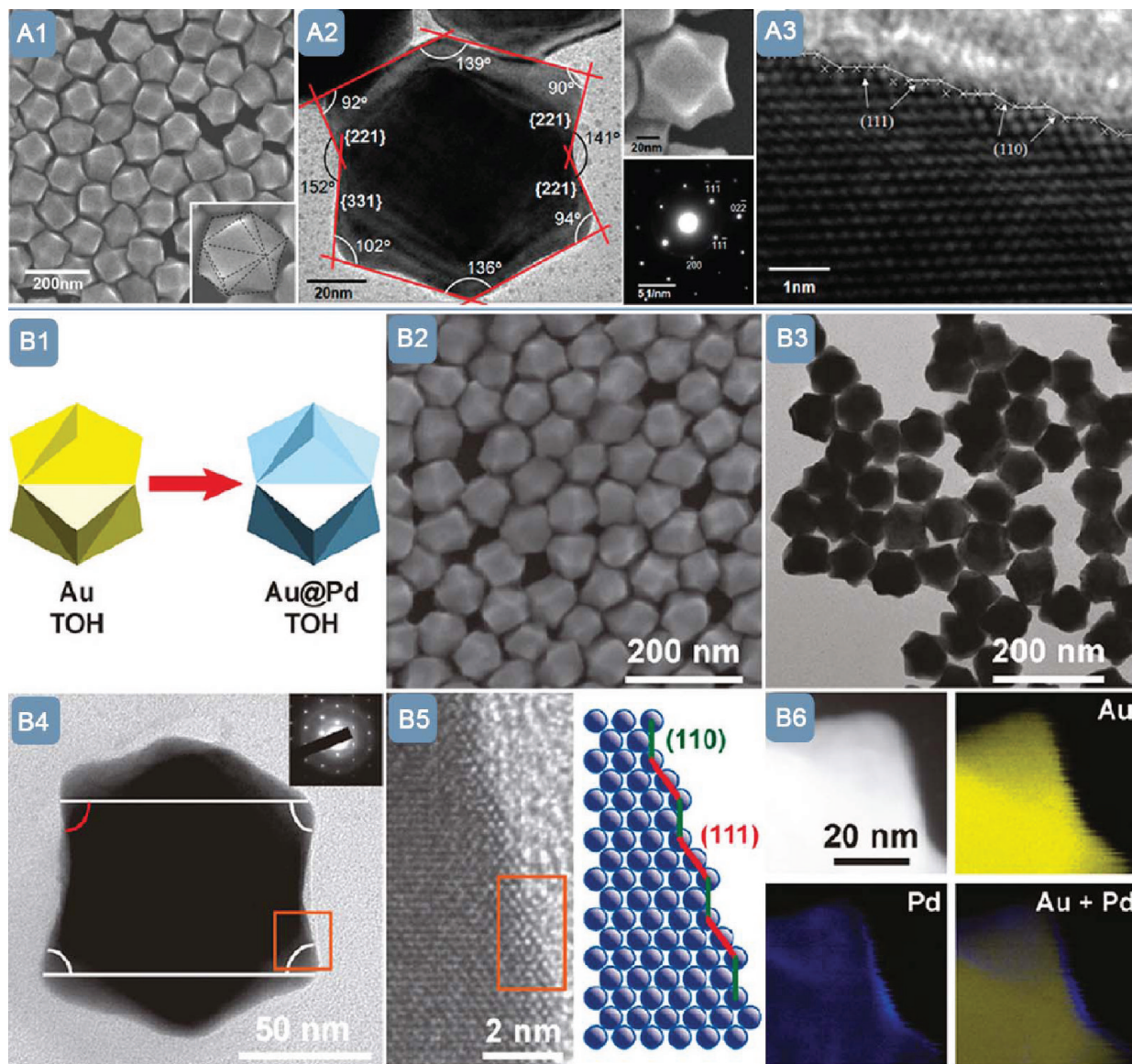


FIGURE 3. Typical cases of $\{hhl\}$ facets. (A1) SEM image of Au TOH; (A2) TEM image, SEM image, and SAED pattern of one Au TOH; (A3) HR-TEM image of Au TOH particle edge; (B1) formation scheme, (B2) SEM image, (B3, B4) TEM images, (B5) HR-TEM image, and (B6) HAADF-STEM image and elemental mapping images of Au–Pd core–shell TOH. (A) Adapted with permission from ref 39. Copyright 2010 American Chemical Society. (B) Adapted with permission from ref 35. Copyright 2011 American Chemical Society.

TOH NCs using Au TOH as starting cores (Figure 3B1).³⁵ By using SEM (Figure 3B2), TEM (Figure 3B3) and high-angle annular dark-field scanning transmission electron microscopy (HAADF-STEM) element mapping (Figure 3B6), the geometry and composition of a Au–Pd TOH core–shell were studied, indicating a Pd shell with a thickness of ~ 15 nm. The exposed surfaces were indexed to $\{221\}$ facets using aforementioned methods (Figure 3B4, method 2; Figure 3B5, method 1). Since the concave nanocube, an inverse structure of THH, is a class of polyhedra bounded with $\{hko\}$ facets, it is expected that the surface planes of concave octahedra (reversed TOH) should be similarly

comprised of $\{hhl\}$ facets. Although $\{100\}$ facets as the depressed surfaces were identified on concave nanooctahedra of Au–Pd core–shell NCs,³⁶ $\{hhl\}$ -terminated concave nanooctahedra are still expected to be found in the near future. In contrast to Au–Pd core–shells as “common” structures, recently Pd–Au core–shell TOH NCs were also successfully synthesized when Pd nanocubes were used as structure-directing cores.⁴⁰

3.3. $\{hkk\}$ Facets. Compared with $\{hk0\}$ and $\{hhl\}$ facets, there has been few reports on synthesis of $\{hkk\}$ -terminated NCs.^{23,37,41,42} Figure 4A1,A2 shows representative $\{hkk\}$ -bounded Pd TPH NCs prepared via an electrochemical

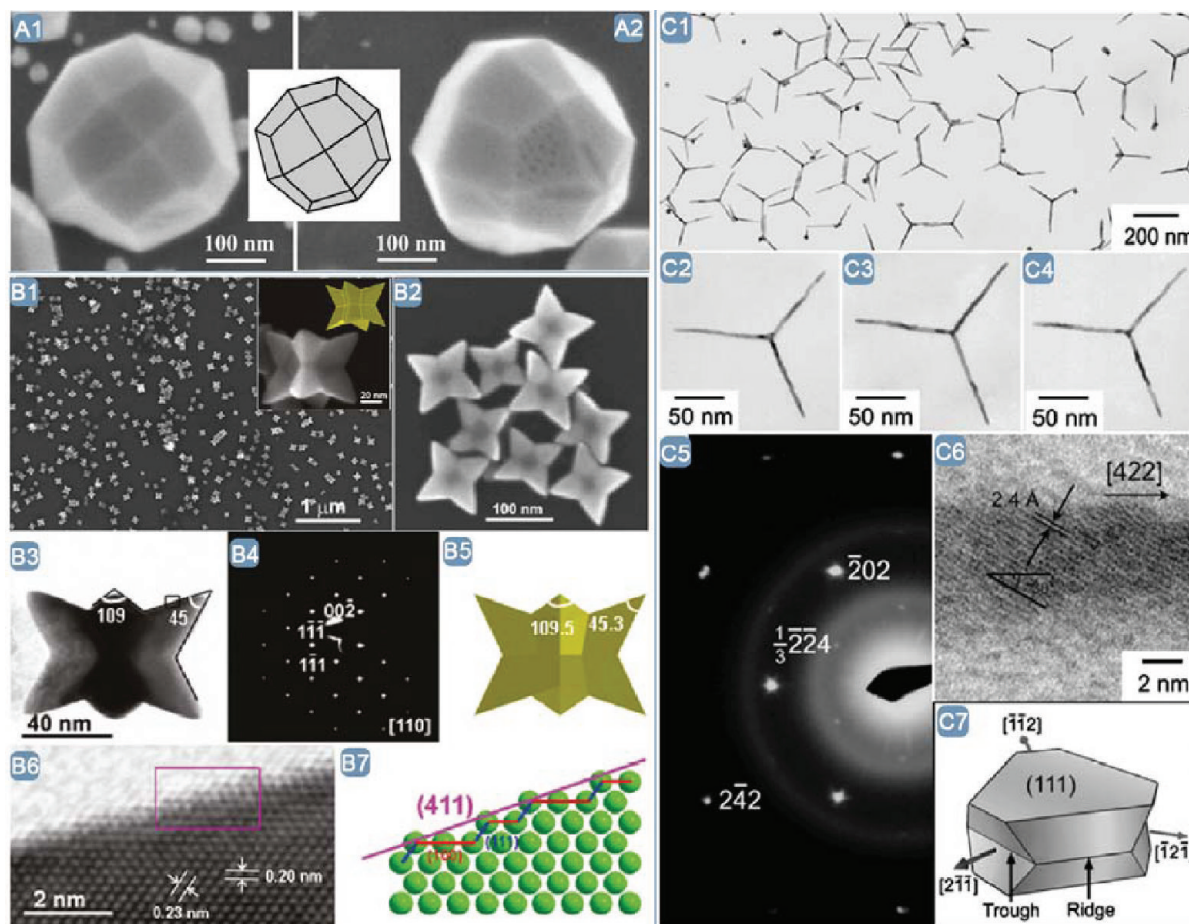


FIGURE 4. Typical cases of $\{hkk\}$ facets. (A1, A2) SEM images of Pd TPH; (B1, B2) SEM images, (B3) TEM image, (B4) SAED pattern, (B5) projection model, and (B6) HR-TEM image of concave Pt NCs with octapod morphology and (B7) atomic model of Pt (411) facet; (C1) TEM image, (C2–C4) TEM images at tilted angles, (C5) SAED pattern, (C6) HR-TEM image, and (C7) growth scheme of Pt planar tripods. (A) Adapted from ref 37. Copyright 2009 The Royal Society of Chemistry. (B) Adapted with permission from ref 42. Copyright 2011 American Chemical Society. (C) Adapted from ref 41. Copyright 2006 The Royal Society of Chemistry.

method.³⁷ Zheng et al. recently reported a synthesis of $\{hkk\}$ -bounded Pt octapods that can be considered as an inverse form of TPH, just like the relationship between concave cube and THH or that between concave octahedron and TOH.⁴² SEM observation (Figure 4B1,B2) indicated that such an octapod structure can be described by excavating out a tetragonal pyramid from each square (100) face of a cube. When these octapod NCs were oriented along the [110] zone axis, they appeared as elongated six-armed stars with four long and two short arms (Figure 4B3). Their exposed surfaces were dominated by $\{411\}$ facets on the basis of determination of several related apex angles (method 2). It was further confirmed (method 1), with an HR-TEM image (Figure 4B6), that the edge-on surfaces were made of subfacets of three (111) and one (100) planes, matching the $\{411\}$ atomic model well (Figure 4B7). Therefore, each cut-out pyramid has a square (100) base face and

four exposed (411) faces passing through the four corners of the excavated (100) square faces.

High-index $\{hkk\}$ facets have also been observed on nanorod surfaces of both Pd 5-fold twinned nanorods²³ and Pt planar tripods.⁴¹ In the former case, the nanorod tip keeps the shape of a pentagonal pyramid with tapers being steeper, while the tip of an $\{hk0\}$ -bounded nanorod changes from a pentagonal pyramid into a decagonal pyramid. Such two similar structures were selectively obtained by controlling the potential limit of square wave.²³ In the latter case, the planar tripods rather than 3D tetrapods were identified by an SEM investigation at different tilted angles (Figure 4C1–C4). Further analysis of SAED and HR-TEM image (Figure 4C5–C7) revealed that three branches actually consist of $\{211\}$ facets. The formation of tripods was believed to be primarily driven by crystal twinning in the (111) plane of Pt.⁴¹

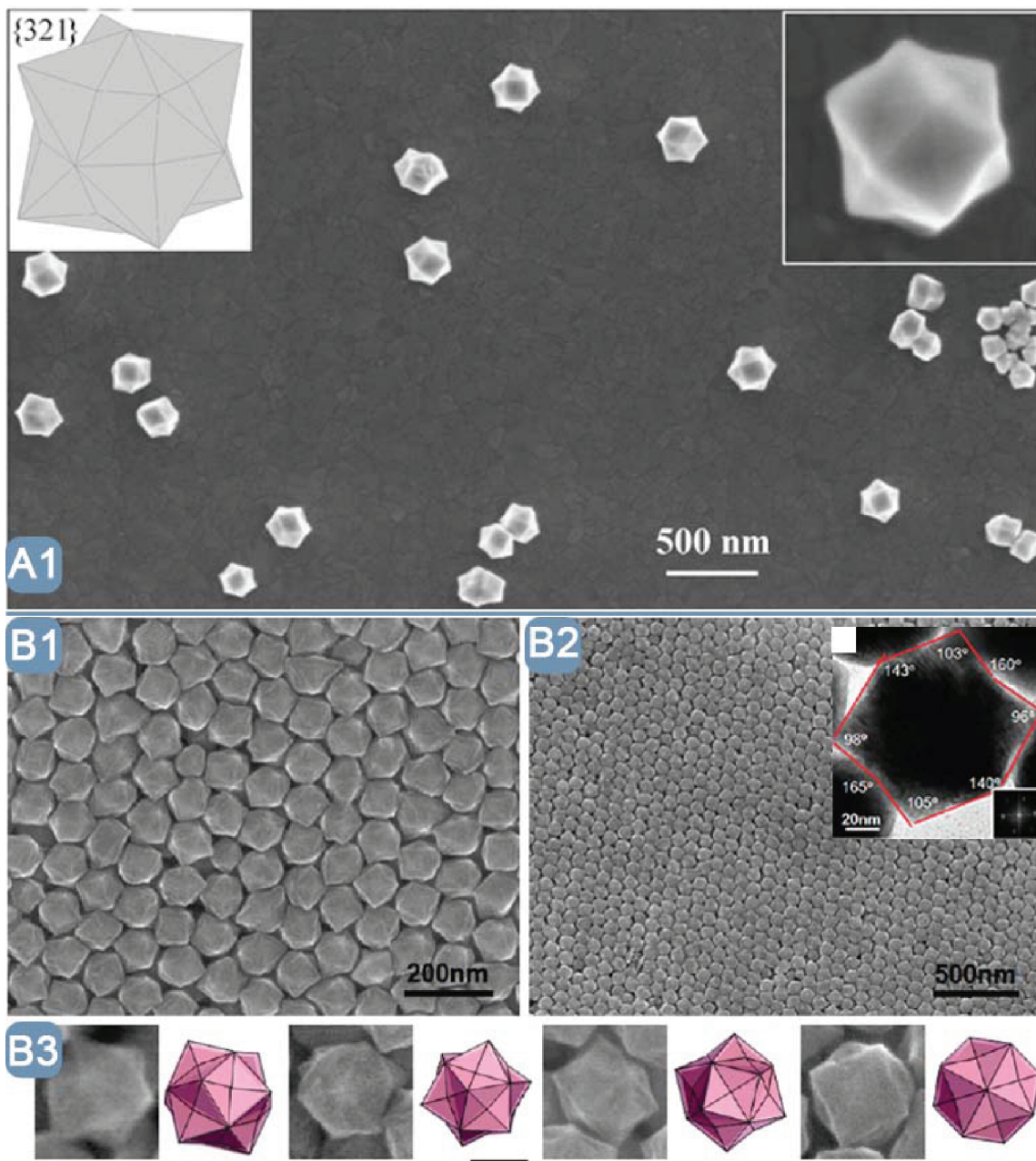


FIGURE 5. Typical cases of $\{hkl\}$ facets. (A1) SEM image of Pd HOH NCs; (B1–B3) SEM images of Au–Pd HOH NCs. Inset of B2 shows a TEM image of one Au–Pd HOH particle. (A) Adapted from ref 37. Copyright 2009 The Royal Society of Chemistry. (B) Adapted with permission from ref 43. Copyright 2011 American Chemical Society.

3.4. $\{hkl\}$ Facets. HOH is known as one representative polyhedron bounded by 48 $\{hkl\}$ facets. It can be visualized as a TOH with each $\langle 111 \rangle$ edge bending outward from the center. Meanwhile, it can also be seen as a THH with each $\langle 100 \rangle$ edge contracting inward from the center. As a result, either each $\{h'h'l'\}$ facet in TOH or each $\{h'k'o\}$ facet in THH is split into two $\{hkl\}$ facets, and therefore the number of $\{hkl\}$ facets in HOH is twice that in TOH and TPH.

As the first demonstration of $\{hkl\}$ -bounded HOH, Pt NCs prepared using a square-wave electrochemical method are

shown in Figure 5A1.³⁷ Lee et al. also demonstrated a fabrication of Au–Pd core–shell HOH NCs.²⁰ SEM images of these NCs (Figure 5B1–B3) matched the TOH model well, and their surface planes were indexed to $\{432\}$ facets according to the measurement of projection angles under the $[110]$ axis (method 2). Such a $\{432\}$ facet can be expressed in terms of the step notation as $2(111) \times (210)$, in which the step itself is a high-index (210) subfacet and thus the atomic arrangement on the edge-on facets (method 1) cannot be used to derive their Miller indices.

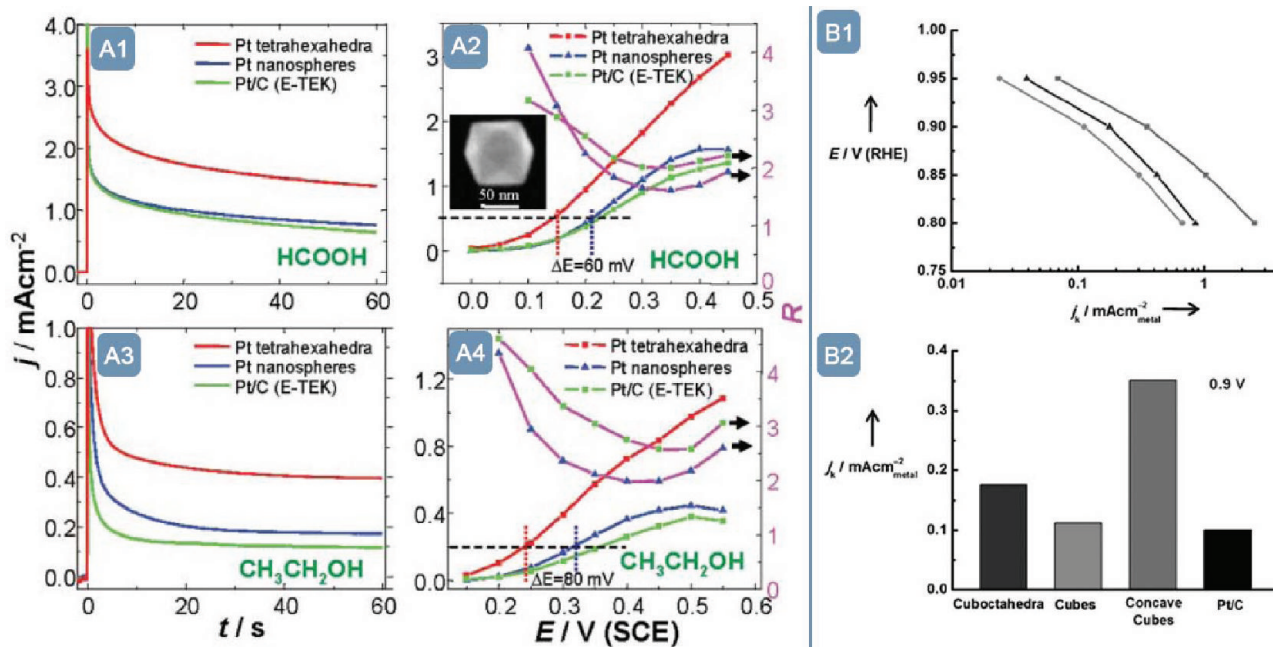


FIGURE 6. Comparison of catalytic activity per unit Pt surface area among THH Pt NCs, polycrystalline Pt nanospheres, and 3.2-nm Pt/C catalyst. (A1 and A3) Transient current density curves of formic acid oxidation at 0.25 V and ethanol oxidation at 0.30 V, respectively; (A2 and A4) potential-dependent steady-state current density (left, recorded at 60 s) and the ratios R (right) between that of THH and the latter two of formic acid oxidation and ethanol oxidation, respectively; (B1) specific activities of the Pt concave cubes (■), cubes (●), and cuboctahedra (▲) toward ORR; (B2) specific activities of these catalysts and Pt/C at 0.9 V versus RHE. (A) Adapted with permission from ref 19. Copyright 2007 American Association for the Advancement of Science. (B) Adapted with permission from ref 30. Copyright 2011 Wiley.

In addition to above core–shell structure, AuPd alloy HOH NCs were prepared by Xie et al.⁴³ with the assistance of Cu^{2+} UPD. The exposed surface planes were indexed to 48 {431} facets based on the outlines and angles between edges of an individual NC (method 2).

4. Enhanced Catalytic Properties by High-Index Facets

One of the most important applications for noble metals is to serve as catalysts in various reactions. It was found that catalytic behavior is highly dependent on surface structure of a catalyst, and a noble metal with appropriate high-index surfaces could offer superior catalytic performance in the bulk state. By sharing this insight, noble metal NCs surrounded by high-index facets could possess further enhanced catalytic properties in comparison with their low-indexed counterparts toward the following selected reactions.

The electrooxidation of small organic molecules (SOMs), including alcohol and formic acid, is an anodic reaction in some fuel cells such as a proton-exchange membrane fuel cell (PEMFC). It was shown that high-indexed noble metal nanopolyhedra could improve their catalytic behaviors toward these reactions, compared with commercial catalyst

with low-index facets. Sun et al. demonstrated how high-indexed NCs could promote the catalytic properties using Pt THH NCs mainly enclosed by {730} facets.¹⁹ In electrochemical catalytic reactions, an electroactive-surface-area normalized current density is usually used to represent catalytic activity for a specific reaction. As presented in Figure 6, the normalized current density on Pt THH NCs enclosed by {730} facets was obviously higher than those on Pt nanospheres and commercial Pt/carbon catalyst¹⁹ toward a formic acid oxidation reaction (Figure 6A1,A2) and an ethanol oxidation reaction (Figure 6A3,A4). Similar improvement was also achieved in other high-indexed Pt NCs such as {411}-enclosed Pt octapods toward these two oxidation reactions.⁴² Additionally, a comparative ethanol oxidation study using carbon-supported 5 nm Pt NCs with multiple high-index facets and 3 nm commercial Pt/carbon NPs implied that the former has superior performance including specific activity, stability, and selectivity.³⁸ In addition to Pt, it was reported that 5-fold twinned Pd nanorods terminated with {hkk} facets²³ and Pd THH bounded with {730} facets²⁴ exhibit 2–3 times and 4–6 times higher specific activity, respectively, than that of commercial Pd black catalyst toward ethanol oxidation in an alkaline solution. It should be noted that the sizes of catalysts should be similar in order

to better compare and evaluate the surface effect on catalytic activity. However, it is still very difficult to obtain nanocatalysts simultaneously with desired size and morphology to date. This is especially the case for the high-index faceted NCs, since these NCs are often obtained by delicately controlling the growth stage. Therefore, most catalytic performance comparisons between the high-index and low-index faceted nanocatalysts have not been based on exactly the same size particles.

Presently, slow oxygen reduction reaction (ORR) rate on the cathode is a major challenge in PEMFCs, whereas nanocatalysts with high-index facets might practically improve the rate.¹⁰ For example, it was reported that the specific activity toward ORR on {720}-bounded Pt concave nanocubes was 3.1–4.1 and 1.9–2.8 times higher than that of low-indexed Pt nanocubes and Pt nanocuboctahedra, respectively, with a similar size³⁰ (Figure 6B1,B2).

Suzuki coupling reaction is another measurement to evaluate the crystal facet-dependent chemical catalysis. As one example, biphenyl could be generated by coupling phenylboronic acid with iodobenzene in the presence of Pd catalyst. Such a “model reaction” can be adopted to determine the performances of high-indexed Pd and Au–Pd core–shell NCs. For instance, {730}-terminated Pd concave nanocubes could amazingly give a yield as high as 99% in 20 min, in comparison with a yield of 38% on Pd nanocubes.²⁹

5. Summary and Outlook

In this Account, we present a collection of noble metal NCs with different classes of high-index facets. In comparison with their low-index surrounded counterparts, such high-indexed NCs exhibit special surface structures that generally correlate to superior catalytic performances toward both electrochemical and chemical reactions. However, there are still some challenges in the near future. First, a synthesis of shape-controlled NCs with high-index facets should be widely explored, since the NC preparations with {*hhl*} (*h* > *l* > 0), {*hkk*} (*h* > *k* > 0), and {*hkl*} (*h* > *k* > *l* > 0) facets are relatively less studied compared with those with {*hk0*} (*h* > *k* > 0) facets. Second, a preservation of high-index facets when reducing the NC size should be extensively investigated in order to increase the mass activity of the electrocatalysts. Finally, the “model reactions” currently being investigated are very limited. In fact, noble metals as catalysts could be alternatively applied to many other fields including fine chemical catalysis (such as hydrogenation of some unsaturated hydrocarbons), the petrochemical industry,

and automobile exhaust pollution treatment. It is expected that these studies will considerably benefit from the design and synthesis of noble metal nanopolyhedra with specific high-index facets as the next generation of advanced materials.

We thank all of the co-workers who have contributed to this field as cited, with special thanks to Liang Li and Prof. Guangwen Zhou for constructing atomic models of the terrace-stepped structures. This work was partially supported by General Motors LLC, Department of Energy and State University of New York at Binghamton.

BIOGRAPHICAL INFORMATION

Zewei Quan was born in Luoyang, China, in 1982. After obtaining his B.Sc. degree in Chemistry from Wuhan University in 2004, he received his Ph.D. degree in Inorganic Chemistry from Changchun Institute of Applied Chemistry, Chinese Academy of Sciences (with Prof. Jun Lin) in 2009. He was a postdoctoral fellow and now is a research scientist in Department of Chemistry at the State University of New York at Binghamton. His current research interests include solution-phase synthesis, self-assembly, and energy conversion of nanostructured materials.

Yuxuan Wang was born in Beijing, China in 1984. He received his B.Sc. degree in Material Science and Engineering from Tsinghua University in 2007. He is now conducting Ph.D. research in the Material Science and Engineering program at the State University of New York at Binghamton. His current research work focuses on shape-controlled synthesis of Pt-based nanomaterials and their potential applications.

Jiye Fang is currently an Associate Professor of Chemistry and director of Materials Science Program/Track, State University of New York at Binghamton. After he graduated from Lanzhou University, he received his M.Sc. in Chemistry and Ph.D. in Materials Science from National University of Singapore in 1994 and 1998, respectively. He was a postdoctoral fellow and subsequently a research specialist in Advanced Materials Research Institute, before joining the Chemistry Department at University of New Orleans as an Assistant Professor in 2002. He was an NSF CAREER award winner. His research direction is shape-controlled synthesis of functional nanomaterials.

FOOTNOTES

*Corresponding author. E-mail: jfang@binghamton.edu.
The authors declare no competing financial interest.

REFERENCES

- Sau, T. K.; Rogach, A. L. Nonspherical Noble Metal Nanoparticles: Colloid-Chemical Synthesis and Morphology Control. *Adv. Mater.* **2010**, *22*, 1781–1804.
- Tian, N.; Zhou, Z.-Y.; Sun, S.-G. Platinum Metal Catalysts of High-Index Surfaces: From Single-Crystal Planes to Electrochemically Shape-Controlled Nanoparticles. *J. Phys. Chem. C* **2008**, *112*, 19801–19817.
- Zhou, Z.-Y.; Tian, N.; Li, J.-T.; Broadwell, I.; Sun, S.-G. Nanomaterials of High Surface Energy with Exceptional Properties in Catalysis and Energy Storage. *Chem. Soc. Rev.* **2011**, *40*, 4167–4185.
- Skrabalak, S. E.; Chen, J.; Sun, Y.; Lu, X.; Au, L.; Cobley, C. M.; Xia, Y. Gold Nanocages: Synthesis, Properties, and Applications. *Acc. Chem. Res.* **2008**, *41*, 1587–1595.

- 5 Wiley, B.; Sun, Y.; Xia, Y. Synthesis of Silver Nanostructures with Controlled Shapes and Properties. *Acc. Chem. Res.* **2007**, *40*, 1067–1076.
- 6 Kim, F.; Connor, S.; Song, H.; Kuykendall, T.; Yang, P. Platonic Gold Nanocrystals. *Angew. Chem., Int. Ed.* **2004**, *43*, 3673–3677.
- 7 Xia, Y.; Xiong, Y.; Lim, B.; Skrabalak, S. E. Shape-Controlled Synthesis of Metal Nanocrystals: Simple Chemistry Meets Complex Physics? *Angew. Chem., Int. Ed.* **2009**, *48*, 60–103.
- 8 Murray, R. W. Nanoelectrochemistry: Metal Nanoparticles, Nanoelectrodes, and Nanopores. *Chem. Rev.* **2008**, *108*, 2688–2720.
- 9 Tao, A. R.; Habas, S.; Yang, P. Shape Control of Colloidal Metal Nanocrystals. *Small* **2008**, *4*, 310–325.
- 10 Stamenkovic, V. R.; Mun, B. S.; Arenz, M.; Mayrhofer, K. J. J.; Lucas, C. A.; Wang, G.; Ross, P. N.; Markovic, N. M. Trends in Electrocatalysis on Extended and Nanoscale Pt-Bimetallic Alloy Surfaces. *Nat. Mater.* **2007**, *6*, 241–247.
- 11 Wang, D.; Peng, Q.; Li, Y. Nanocrystalline Intermetallics and Alloys. *Nano Res.* **2010**, *3*, 574–580.
- 12 Xu, D.; Bliznakov, S.; Liu, Z.; Fang, J.; Dimitrov, N. Composition-Dependent Electrocatalytic Activity of Pt-Cu Nanocube Catalysts for Formic Acid Oxidation. *Angew. Chem., Int. Ed.* **2010**, *49*, 1282–1285.
- 13 Zhang, J.; Yang, H.; Fang, J.; Zou, S. Synthesis and Oxygen Reduction Activity of Shape-Controlled Pt₃Ni Nanopolyhedra. *Nano Lett.* **2010**, *10*, 638–644.
- 14 Zhang, J.; Fang, J. A General Strategy for Preparation of Pt 3d-Transition Metal (Co, Fe, Ni) Nanocubes. *J. Am. Chem. Soc.* **2009**, *131*, 18543–18547.
- 15 Van Santen, R. A. Complementary Structure Sensitive and Insensitive Catalytic Relationships. *Acc. Chem. Res.* **2008**, *42*, 57–66.
- 16 Wang, Z. L. Transmission Electron Microscopy of Shape-Controlled Nanocrystals and Their Assemblies. *J. Phys. Chem. B* **2000**, *104*, 1153–1175.
- 17 Faraday, M. The Bakerian Lecture: Experimental Relations of Gold (and Other Metals) to Light. *R. Soc. London Philos. Trans.* **1857**, *147*, 145–181.
- 18 Ahmadi, T. S.; Wang, Z. L.; Green, T. C.; Henglein, A.; El-Sayed, M. A. Shape-Controlled Synthesis of Colloidal Platinum Nanoparticles. *Science* **1996**, *272*, 1924–1925.
- 19 Tian, N.; Zhou, Z.-Y.; Sun, S.-G.; Ding, Y.; Wang, Z. L. Synthesis of Tetrahedral Platinum Nanocrystals with High-Index Facets and High Electro-Oxidation Activity. *Science* **2007**, *316*, 732–735.
- 20 Yu, Y.; Zhang, Q.; Liu, B.; Lee, J. Y. Synthesis of Nanocrystals with Variable High-Index Pd Facets through the Controlled Heteroepitaxial Growth of Trisuboctahedral Au Templates. *J. Am. Chem. Soc.* **2010**, *132*, 18258–18265.
- 21 Lang, B.; Joyner, R. W.; Somorjai, G. A. Low Energy Electron Diffraction Studies of Chemisorbed Gases on Stepped Surfaces of Platinum. *Surf. Sci.* **1972**, *30*, 454–474.
- 22 Van Hove, M. A.; Somorjai, G. A. A New Microfacet Notation for High-Miller-Index Surfaces of Cubic Materials with Terrace, Step and Kink Structures. *Surf. Sci.* **1980**, *92*, 489–518.
- 23 Tian, N.; Zhou, Z.-Y.; Sun, S.-G. Electrochemical Preparation of Pd Nanorods with High-Index Facets. *Chem. Commun.* **2009**, 1502–1504.
- 24 Tian, N.; Zhou, Z.-Y.; Yu, N.-F.; Wang, L.-Y.; Sun, S.-G. Direct Electrodeposition of Tetrahedral Pd Nanocrystals with High-Index Facets and High Catalytic Activity for Ethanol Electrooxidation. *J. Am. Chem. Soc.* **2010**, *132*, 7580–7581.
- 25 Ma, Y.; Kuang, Q.; Jiang, Z.; Xie, Z.; Huang, R.; Zheng, L. Synthesis of Trisuboctahedral Gold Nanocrystals with Exposed High-Index Facets by a Facile Chemical Method. *Angew. Chem., Int. Ed.* **2008**, *47*, 8901–8904.
- 26 Ming, T.; Feng, W.; Tang, Q.; Wang, F.; Sun, L.; Wang, J.; Yan, C. Growth of Tetrahedral Gold Nanocrystals with High-Index Facets. *J. Am. Chem. Soc.* **2009**, *131*, 16350–16351.
- 27 Nikoobakht, B.; El-Sayed, M. A. Preparation and Growth Mechanism of Gold Nanorods (NRs) Using Seed-Mediated Growth Method. *Chem. Mater.* **2003**, *15*, 1957–1962.
- 28 Sau, T. K.; Murphy, C. J. Seeded High Yield Synthesis of Short Au Nanorods in Aqueous Solution. *Langmuir* **2004**, *20*, 6414–6420.
- 29 Jin, M.; Zhang, H.; Xie, Z.; Xia, Y. Palladium Concave Nanocubes with High-Index Facets and Their Enhanced Catalytic Properties. *Angew. Chem., Int. Ed.* **2011**, *50*, 7850–7854.
- 30 Yu, T.; Kim, D. Y.; Zhang, H.; Xia, Y. Platinum Concave Nanocubes with High-Index Facets and Their Enhanced Activity for Oxygen Reduction Reaction. *Angew. Chem., Int. Ed.* **2011**, *50*, 2773–2777.
- 31 Zhang, J.; Langille, M. R.; Personick, M. L.; Zhang, K.; Li, S.; Mirkin, C. A. Concave Cubic Gold Nanocrystals with High-Index Facets. *J. Am. Chem. Soc.* **2010**, *132*, 14012–14014.
- 32 Liu, M.; Guyot-Sionnest, P. Mechanism of Silver(I)-Assisted Growth of Gold Nanorods and Bipyramids. *J. Phys. Chem. B* **2005**, *109*, 22192–22200.
- 33 Personick, M. L.; Langille, M. R.; Zhang, J.; Mirkin, C. A. Shape Control of Gold Nanoparticles by Silver Underpotential Deposition. *Nano Lett.* **2011**, *11*, 3394–3398.
- 34 Tran, T. T.; Lu, X. Synergistic Effect of Ag and Pd Ions on Shape-Selective Growth of Polyhedral Au Nanocrystals with High-Index Facets. *J. Phys. Chem. C* **2011**, *115*, 3638–3645.
- 35 Wang, F.; Li, C.; Sun, L.-D.; Wu, H.; Ming, T.; Wang, J.; Yu, J. C.; Yan, C.-H. Heteroepitaxial Growth of High-Index-Faceted Palladium Nanoshells and Their Catalytic Performance. *J. Am. Chem. Soc.* **2011**, *133*, 1106–1111.
- 36 Lu, C.-L.; Prasad, K. S.; Wu, H.-L.; Ho, J.-a. A.; Huang, M. H. Au Nanocube-Directed Fabrication of Au–Pd Core–Shell Nanocrystals with Tetrahedral, Concave Octahedral, and Octahedral Structures and Their Electrocatalytic Activity. *J. Am. Chem. Soc.* **2010**, *132*, 14546–14553.
- 37 Zhou, Z.-Y.; Tian, N.; Huang, Z.-Z.; Chen, D.-J.; Sun, S.-G. Nanoparticle Catalysts with High Energy Surfaces and Enhanced Activity Synthesized by Electrochemical Method. *Farad. Discuss.* **2009**, *140*, 81–92.
- 38 Zhou, Z.-Y.; Huang, Z.-Z.; Chen, D.-J.; Wang, Q.; Tian, N.; Sun, S.-G. High-Index Faceted Platinum Nanocrystals Supported on Carbon Black as Highly Efficient Catalysts for Ethanol Electrooxidation. *Angew. Chem., Int. Ed.* **2010**, *49*, 411–414.
- 39 Yu, Y.; Zhang, Q.; Lu, X.; Lee, J. Y. Seed-Mediated Synthesis of Monodisperse Concave Trisuboctahedral Gold Nanocrystals with Controllable Sizes. *J. Phys. Chem. C* **2010**, *114*, 11119–11126.
- 40 Zhang, L.; Niu, W.; Li, Z.; Xu, G. Facile Synthesis and Electrochemiluminescence Application of Concave Trisuboctahedral Pd@Au Core-Shell Nanocrystals Bound by {331} High-Index Facets. *Chem. Commun.* **2011**, 10353–10355.
- 41 Maksimuk, S.; Teng, X.; Yang, H. Planar Tripods of Platinum: Formation and Self-Assembly. *Phys. Chem. Chem. Phys.* **2006**, *8*, 4660–4663.
- 42 Huang, X.; Zhao, Z.; Fan, J.; Tan, Y.; Zheng, N. Amine-Assisted Synthesis of Concave Polyhedral Platinum Nanocrystals Having {411} High-Index Facets. *J. Am. Chem. Soc.* **2011**, *133*, 4718–4721.
- 43 Zhang, L.; Zhang, J.; Kuang, Q.; Xie, S.; Jiang, Z.; Xie, Z.; Zheng, L. Cu²⁺-Assisted Synthesis of Hexoctahedral Au–Pd Alloy Nanocrystals with High-Index Facets. *J. Am. Chem. Soc.* **2011**, *133*, 17114–17117.